Investigations into critical earthquake load models within deterministic and probabilistic frameworks

A. M. Abbas[†] and C. S. Manohar[*,‡]

Department of Civil Engineering, Indian Institute of Science, Bangalore 560012, India

SUMMARY

This paper deals with the determination of critical earthquake load models for linear structures subjected to single-point seismic inputs. The primary objective of this study is to examine the realism in critical excitations and critical responses *vis a vis* the framework adopted for the study and constraints that these excitations are taken to satisfy. Two alternative approaches are investigated. In the first approach, the critical earthquake is expressed in terms of a Fourier series that is modulated by an enveloping function that imparts transient nature to the inputs. The Fourier coefficients are taken to be deterministic and are constrained to satisfy specified upper and lower bounds. Estimates on these bounds, for a given site, are obtained by analysing past earthquake records from the same site or similar sites. The unknown Fourier coefficients are determined such that the response of a given structure is maximized subjected to these bounds and additional constraints on intensity, peak ground acceleration, peak ground velocity and peak ground displacement. In the second approach, the critical earthquake is modelled as a partially specified non-stationary Gaussian random process which is defined in terms of a stationary random process of unknown power spectral density (psd) function modulated by a deterministic envelope function. The input is constrained to possess specified variance and average zero crossing rate. Additionally, a new constraint in terms of entropy rate representing the expected level of disorder in the excitation is also imposed. The unknown psd function of the stationary part of the input is determined so that the response of a given structure is maximized. The optimization problem in both these approaches is solved by using sequential quadratic programming method. The procedures developed are illustrated by considering the seismic response of a tall chimney and an earth dam. It is concluded that the imposition of lower and upper bounds on Fourier coefficients in the first approach and constraints on amount of disorder in the second approach are crucial in arriving at realistic critical excitations. Copyright © 2002 John Wiley & Sons, Ltd.

KEY WORDS: critical earthquake excitations; random vibrations; entropy rate

1. INTRODUCTION

The method of seismic critical excitations provides a framework to deal with seismic response of engineering structures subjected to inadequately specified earthquake input. Given

---

[*] Correspondence to: C. S. Manohar, Department of Civil Engineering, Indian Institute of Science, Bangalore 560012, India.
[†] E-mail: abbas@civil.iisc.ernet.in
[‡] E-mail: manohar@civil.iisc.ernet.in

the general paucity of data on strong motion ground accelerations on one hand and require-
ments on design for low risks of important structures on the other, this method is of con-
siderable interest in earthquake engineering. Thus, for instance, for the region of peninsular
India, there are hardly few strong motion records available for the 1993 Khilari earthquake
and the 2001 Bhuj earthquake. To the best of authors' knowledge, there are no strong mo-
tion data available for the main shock for these earthquakes. The method of critical ex-
citation has its roots in the field of electrical engineering and was introduced to the field
of earthquake engineering by Drenick [1, 2]. A brief chronology of selected literature pub-
lished prior to 1995 has been presented by Manohar and Sarkar [3]. The central idea of this
method consists of optimizing the missing information in the inputs such that a chosen re-
sponse variable of a given structure is maximized. Consequently, these optimal excitations,
not only embody partial information that is readily available on the earthquake inputs, but
also, are tailored according to the dynamic characteristics of the structure under consideration
so that these excitations produce the highest response. The available methods for finding crit-
ical excitations can be schematized based on the following alternative criteria: (a) whether
the excitations are deterministic or stochastic, (b) whether multiple components and spatial
variability are accounted for or not, (c) whether excitations are described in terms of time
history/response spectra or via psd function and (d) whether system being considered is
linear/non-linear or singly supported/multiply supported. However, for the purpose of discus-
sion of this paper, the available methods for determining critical earthquakes can be classi-
fied into three categories, namely, data-based models, parametric models and non-parametric
models.

In the data-based models, a set of time histories of earthquakes recorded in the given site
or on geologically similar sites are used as basis functions in defining the critical excitations
[2, 4]. Thus the formulation proposed by Drenick [2], Wang and Yun [4] and Bedrosian *et
al.* [5] represent the critical excitations as a linear combination of the basis records and the
coefficients of this expansion are optimized to produce highest response under constraints on
earthquake intensity and peak ground acceleration. The main advantage of this method is that
the frequency content of earthquake ground motion is well-represented. The basic premise that
past earthquake records serve as basis functions to represent future earthquakes is, however,
questionable, since there is no reason why past records need to form a complete set. There-
fore, the questions on convergence of the series representation become difficult to answer.
The study by Srinivasan *et al.* [6] is representative of parametric critical excitation models.
These authors modelled the earthquake acceleration as a non-stationary filtered shot noise and
optimized the parameters of this model such that response of a given system is maximized. In
this study, the use of a specific model for earthquake loads provided a constraint on nature of
excitation. The earlier study by Drenick [1], in which he showed that critical excitations for
linear systems are given by their impulse response functions reversed in time, is an example
for non-parametric models. Shinozuka [7] solved the same problem by introducing an upper
bound on the Fourier amplitude spectrum of the critical excitation. Similarly, the studies on
determination of stochastic critical excitations reported by Iyengar and Manohar [8], Manohar
and Sarkar [3], Sarkar and Manohar [9, 10] and Takewaki [11, 12] provide examples of non-
parametric models within the probabilistic framework. In these studies, the input processes are
taken to be Gaussian and the functional form of the critical psd function/matrix are determined
by maximizing the structure responses. One of the deficiencies in critical psd function/matrix
models developed so far has been that these critical excitations tend to be resonant in nature

and often produce overly conservative responses. Clearly, there exists a need to device suitable constraints that would produce critical excitations that have realistic frequency content and thereby display the disorder characteristics which recorded earthquakes ground motion possess.

The present study develops two alternative ways to arrive at critical earthquake excitations. The structures considered are taken to be linear and all supports are assumed acted upon by a single horizontal ground motion. The first method that is considered is in the spirit of the data-based models [2, 4, 5] but with a significant difference. Instead of representing the critical earthquake as a linear combination of past recorded earthquakes, it is now represented by a product of an enveloping function and a steady-state function that can be represented by a Fourier series. The data available on past earthquakes are used to construct upper and lower bounds on the Fourier amplitude spectra, which, in turn, are imposed as constraints in deriving critical excitations. Additional constraints involving peak ground acceleration, peak ground velocity and peak ground displacement are also considered. In the second method that is studied, the critical earthquake is modelled as a non-stationary Gaussian random process that is obtained by multiplying a deterministic modulating envelope function with a stationary Gaussian random process of zero mean. The critical psd of the stationary part of the excitation is taken to be unknown and is required to be found such that structure response is maximized. The constraints that are imposed include limits on input variance and the estimate of the average zero crossing rate. Additionally, the paper proposes a new constraint in terms of entropy rate of the input that reflects the measure of disorder that can be expected in realistic earthquake ground motions. Mathematically, the problem of determining the critical excitation in both these approaches are shown to constitute constrained non-linear optimization problems. Numerical illustrations on critical excitations for a tall chimney and for an earth dam are presented.

2. MODEL I: DETERMINISTIC CRITICAL EARTHQUAKES

The equation of motion for the relative displacement $\mathbf{u}(t)$ of a discretized N-degree-of-freedom linear structure driven by a single component horizontal ground acceleration $\ddot{u}_{\mathrm{g}}(t)$ at its base is given by [13]

$$\mathbf{M}\ddot{\mathbf{u}}(t) + \mathbf{C}\dot{\mathbf{u}}(t) + \mathbf{K}\mathbf{u}(t) = -\mathbf{M}\{\mathbf{1}\}\ddot{u}_{\mathrm{g}}(t) \tag{1}$$

Here $\mathbf{M}, \mathbf{C}, \mathbf{K}$ are, respectively, the mass, damping and stiffness matrices of the discretized structure, and $\{\mathbf{1}\}$ represents a column vector of ones. Assuming the damping to be proportional, and also that system starts from rest, the kth displacement component can be shown to be given by

$$u_k(t) = \sum_{i=1}^{N} \gamma_i \phi_{ki} \int_0^t \ddot{u}_{\mathrm{g}}(\tau) h_i(t-\tau)\, \mathrm{d}\tau; \quad \gamma_i = -\frac{\phi_i^{\mathrm{T}} \mathbf{M}\{\mathbf{1}\}}{\phi_i^{\mathrm{T}} \mathbf{M}\phi_i} \tag{2}$$

where γ_i is the participation factor for the ith mode, ϕ the modal matrix and $h_i(t)$ the ith impulse response function. It may be noted that, in this model, the ground acceleration $\ddot{u}_{\mathrm{g}}(t)$ is taken to be deterministic and is assumed to be represented by

$$\ddot{u}_{\mathrm{g}}(t) = e(t)\ddot{w}_{\mathrm{g}}(t) \tag{3}$$

Here $e(t)$ is an enveloping function that imparts transient nature to the inputs and $\ddot{w}_g(t)$ is a steady-state function that admits a Fourier representation of the form

$$\ddot{w}_g(t) = \sum_{n=1}^{N_f} [A_n \cos \omega_n t + B_n \sin \omega_n t] \tag{4}$$

where A_n and B_n are unknown constants, and the frequencies ω_n, $n = 1, 2, \ldots, N_f$, are selected such that they span satisfactorily the frequency range (ω_0, ω_c). The envelope function $e(t)$ is assumed to be of the form

$$e(t) = A_0[\exp(-\alpha t) - \exp(-\beta t)], \quad \beta > \alpha > 0 \tag{5}$$

Here α and β are parameters that impart the observed transient trends in the recorded ground motions [14]. In our study, we take these parameters to be known and specifically it is assumed that $\alpha = 0.13$ and $\beta = 0.50$. This choice represents the earthquake duration to be about 30 s that is considered typical of magnitude 7.0 earthquake.

In constructing the critical excitation model, it is assumed that $e(t)$ is completely specified and $\{A_n, B_n\}_{n=1}^{N_f}$ are unknowns. Furthermore, the information on intensity E_1, peak ground acceleration (PGA) M_1, peak ground velocity (PGV) M_2, peak ground displacement (PGD) M_3, upper bound Fourier amplitude spectra (UBFAS) $M_4(\omega)$ and lower bound Fourier amplitude spectra (LBFAS) $M_5(\omega)$ are taken to be available which enables the formulation of the following constraints:

$$\left[\int_0^\infty \ddot{u}_g^2(t) \, \mathrm{d}t \right]^{1/2} \leqslant E_1$$

$$\max_{0 < t < \infty} |\ddot{u}_g(t)| \leqslant M_1$$

$$\max_{0 < t < \infty} |\dot{u}_g(t)| \leqslant M_2 \tag{6}$$

$$\max_{0 < t < \infty} |u_g(t)| \leqslant M_3$$

$$M_5(\omega) \leqslant |\ddot{U}_g(\omega)| \leqslant M_4(\omega)$$

Here $\ddot{U}_g(\omega)$ is the Fourier transform of the ground acceleration $\ddot{u}_g(t)$. To proceed further, we need to express the ground velocity and displacement in terms of the Fourier coefficients A_n and B_n. Accordingly, from Equations (3) and (4), one gets

$$\dot{u}_g(t) = \sum_{n=1}^{N_f} \int_0^t e(\tau)[A_n \cos \omega_n \tau + B_n \sin \omega_n \tau] \, \mathrm{d}\tau + C_1 \tag{7}$$

$$u_g(t) = \sum_{n=1}^{N_f} \int_0^t e(\tau)(t - \tau)[A_n \cos \omega_n \tau + B_n \sin \omega_n \tau] \, \mathrm{d}\tau + C_1 t + C_2 \tag{8}$$

The constants of the integrations C_1 and C_2 are found using the conditions [15]

$$u_g(0) = 0, \quad \lim_{t \to \infty} \dot{u}_g(t) \to 0 \tag{9}$$

This leads to

$$C_2 = 0, \quad C_1 = -\sum_{n=1}^{N_f} \int_0^\infty e(\tau)[A_n \cos \omega_n \tau + B_n \sin \omega_n \tau]\, d\tau \tag{10}$$

Subsequently, the constraints listed in Equation (6) can be expressed in terms of A_n and B_n as follows:

$$\left[\sum_{m=1}^{N_f} \sum_{n=1}^{N_f} A_m A_n I_{1mn} + A_m B_n I_{2mn} + B_m A_n I_{3mn} + B_m B_n I_{4mn} \right]^{1/2} \leqslant E_1$$

$$\max_{0 < t < \infty} \left| e(t) \sum_{n=1}^{N_f} [A_n \cos \omega_n t + B_n \sin \omega_n t] \right| \leqslant M_1$$

$$\max_{0 < t < \infty} \left| \sum_{n=1}^{N_f} \int_0^t e(\tau)[A_n \cos \omega_n \tau + B_n \sin \omega_n \tau]\, d\tau \right.$$

$$\left. - \sum_{n=1}^{N_f} \int_0^\infty e(\tau)[A_n \cos \omega_n \tau + B_n \sin \omega_n \tau]\, d\tau \right| \leqslant M_2 \tag{11}$$

$$\max_{0 < t < \infty} \left| \sum_{n=1}^{N_f} \int_0^t e(\tau)(t - \tau)[A_n \cos \omega_n \tau + B_n \sin \omega_n \tau]\, d\tau \right.$$

$$\left. - t \sum_{n=1}^{N_f} \int_0^\infty e(\tau)[A_n \cos \omega_n \tau + B_n \sin \omega_n \tau]\, d\tau \right| \leqslant M_3;$$

$$M_5(\omega) \leqslant \left| \sum_{n=1}^{N_f} A_n I_{1n}(\omega) + B_n I_{2n}(\omega) \right| \leqslant M_4(\omega)$$

where

$$I_{1mn} = \int_0^\infty e^2(t) \cos \omega_m t \cos \omega_n t\, dt; \qquad I_{2mn} = \int_0^\infty e^2(t) \cos \omega_m t \sin \omega_n t\, dt$$

$$I_{3mn} = \int_0^\infty e^2(t) \sin \omega_m t \cos \omega_n t\, dt; \qquad I_{4mn} = \int_0^\infty e^2(t) \sin \omega_m t \sin \omega_n t\, dt \tag{12}$$

$$I_{1n}(\omega) = \int_0^\infty e(t) \cos \omega_n t \exp(-j\omega t)\, dt; \quad I_{2n}(\omega) = \int_0^\infty e(t) \sin \omega_n t \exp(-j\omega t)\, dt; \ j = \sqrt{-1}$$

To determine the quantities $E_1, M_1, M_2, M_3, M_4(\omega)$ and $M_5(\omega)$, it is assumed that a set of earthquake records denoted by $\{\ddot{v}_{gn}(t)\}_{n=1}^{N_r}$ are available for the site under consideration or from other sites that are geologically similar to the given site. The values of intensity, peak values of acceleration, velocity and displacement are obtained for each of these records. The highest of these values across the ensemble of the records are taken to be the respective estimates of E_1, M_1, M_2 and M_3. The set of available records $\{\ddot{v}_{gn}(t)\}_{n=1}^{N_r}$ are further normalized so that the PGA of each record is set to unity, and these normalized records are denoted by $\{\ddot{\bar{v}}_{gn}(t)\}_{n=1}^{N_r}$. The bounds $M_4(\omega)$ and $M_5(\omega)$ are obtained as

$$M_4(\omega) = M_1 \max_{1 \leqslant n \leqslant N_r} |\ddot{\bar{V}}_{gn}(\omega)|$$

$$M_5(\omega) = M_1 \min_{1 \leqslant n \leqslant N_r} |\ddot{\bar{V}}_{gn}(\omega)| \tag{13}$$

Earthquake Engng Struct. Dyn. 2002; **31**:813–832

Here $\{\ddot{\bar{V}}_{gn}(\omega)\}_{n=1}^{N_r}$ denote the Fourier transform of $\{\ddot{\bar{v}}_{gn}(t)\}_{n=1}^{N_r}$ and these transforms are computed using the FFT algorithm. It may be noted that the idea of introducing an upper bound on the Fourier amplitude of the ground motion has been considered earlier by Shinozuka [7], Baratta *et al.* [16] and, also, in a probabilistic setting, by Takewaki [11, 12]. These authors, however, have not considered introducing the lower bound on the Fourier amplitude spectra. It may also be remarked here that the assumption on availability of past records $\{\ddot{v}_{gn}(t)\}_{n=1}^{N_r}$ is similar to the assumption made by Drenick [2]. While the earlier workers [2, 4, 5] employed these records as basis functions, in our study, these records are used to derive the constraints that the critical excitations need to satisfy.

The problem of determining the critical excitation can now be stated as finding $\{A_n, B_n\}_{n=1}^{N_f}$ which maximize

$$\max_{0<t<\infty} |u_k(t)| = \max_{0<t<\infty} \left| \sum_{i=1}^{N} \sum_{n=1}^{N_f} \gamma_i \phi_{ki} \int_0^t e(\tau)[A_n \cos \omega_n \tau + B_n \sin \omega_n \tau] h_i(t-\tau)\, d\tau \right| \qquad (14)$$

subjected to the constraints listed in Equations (11). It is to be noted that this problem constitutes a constrained non-linear optimization problem. The solution to this problem, in our study, is computed using the '*CONSTR*' program that forms a part of the MATLAB Optimization Toolbox. This program, in turn, is based on sequential quadratic optimization method. The steps of the maximization procedures can be summarized as follows:

1. Calculate the impulse response functions, $\{h_i(t_j - \tau)\}_{i=1}^{N}$ at time $t = t_j$.
2. Compute $\{A_n, B_n\}_{n=1}^{N_f}$ that maximize the response $u_k(t_j)$, Equations (2)–(4).
3. Repeat steps 1 and 2 for all time points.
4. Estimate the maximum response $u_k(t_m) = \max |u_k(t_j)|$ and corresponding $\{A_n, B_n\}_{n=1}^{N_f}$.
5. The estimated $\{A_n, B_n\}_{n=1}^{N_f}$ define the critical input (Equations (3) and (4)) and corresponding critical response (Equation (2)).

It may be emphasized that the selection of past records in the above formulation is primarily based on local soil condition. Any new record that brings in changes in the values of the constraints will automatically alter the critical responses. This is an inherent feature of the method. In selecting the values of the constraints, in our study, we have chosen the extreme values instead of average or average + factor of the standard deviation as was done by Bedrosian *et al.* [5]. These values could perhaps be scaled by factors greater than one to account for finite size of the set of records. The procedure for calibration of these scaling factors, however, is not obvious. A more rational alternative is to treat $E_1, M_1, M_2, M_3, M_4(\omega)$ and $M_5(\omega)$ as being stochastic in nature with their probability density functions estimated from the available records. The present study, however, does not consider these aspects.

3. MODEL II: STOCHASTIC CRITICAL EARTHQUAKES

The earthquake ground motion here is modelled as a non-stationary Gaussian random process that is obtained by multiplying a deterministic envelope with a stationary zero mean Gaussian random process. The ground acceleration $\ddot{u}_g(t)$ is again represented as in Equation (3) but

with the important difference that the coefficients $\{A_n, B_n\}_{n=1}^{N_f}$ are now modelled as a vector of zero mean Gaussian random variables that satisfy the conditions:

$$\langle A_m A_n \rangle = \sigma_n^2 \delta_{mn}; \quad \langle B_m B_n \rangle = \sigma_n^2 \delta_{mn}$$

$$\langle A_m B_n \rangle = 0; \quad \forall \; m, n = 1, 2, \ldots, N_f$$

(15)

Here, $\langle \cdot \rangle$ denotes the mathematical expectation operator and δ_{mn} is the Kronecker delta. Under these conditions $\ddot{w}_g(t)$ becomes a stationary Gaussian random process with auto covariance and power spectral density (psd) function given, respectively, by

$$R(\tau) = \sum_{n=1}^{N_f} \sigma_n^2 \cos(\omega_n \tau); \quad S(\omega) = \sum_{n=1}^{N_f} \sigma_n^2 \delta(\omega - \omega_n)$$

(16)

The total average energy E_T and the average rate of zero crossing with positive slopes, n_0^+, can be expressed in terms of $e(t)$ and $S(\omega)$ as follows:

$$E_T = E_0 \int_0^\infty e^2(t) \, \mathrm{d}t; \quad n_0^+ = \frac{1}{2\pi} \sqrt{\frac{E_2}{E_0}}$$

(17)

Here the quantities E_0 and E_2 are the spectral moments of $S(\omega)$ and are given by

$$E_0 = \int_{\omega_0}^{\omega_c} S(\omega) \, \mathrm{d}\omega; \quad E_2 = \int_{\omega_0}^{\omega_c} \omega^2 S(\omega) \, \mathrm{d}\omega$$

(18)

As before, the interval (ω_0, ω_c) represents the frequency range of the ground acceleration. Referring to Equations (1) and (2), and taking into account that $\ddot{u}_g(t)$ is a non-stationary random process, it can be shown that the response variance $\bar{\sigma}_k^2(t)$ at the kth degree of freedom can be written in the following form:

$$\bar{\sigma}_k^2(t) = \int_{\omega_0}^{\omega_c} S(\omega) H_k(\omega, t) \, \mathrm{d}\omega$$

(19)

Here $H_k(\omega, t)$ can be interpreted as the generalized frequency response function for the kth degree-of-freedom and is expressed in terms of the impulse response function, mode shape, participation factor and the excitation envelope function as follows:

$$H_k(\omega, t) = \sum_{i=1}^{N} \sum_{j=1}^{N} \gamma_i \gamma_j \phi_{ki} \phi_{kj} \int_0^t \int_0^t e(\tau_1) e(\tau_2) h_i(t - \tau_1) h_j(t - \tau_2) \cos \omega(\tau_2 - \tau_1) \, \mathrm{d}\tau_1 \, \mathrm{d}\tau_2$$

(20)

In an earlier study [3], critical psd functions that maximize response variance of a given structure subjected to constraints not only on E_T but also on n_0^+ have been determined. Here the constraint on n_0^+ was imposed to reflect the influence of dominant frequency as dictated by the local soil conditions. The resulting critical excitations were, however, found to be narrow banded in nature with most of the average power centred around the structure natural frequency with the soil layer frequency playing no significant role in dictating the average power distribution across the frequency range of interest. To remedy this, Manohar and Sarkar [3] suggested that the 'disorder' that is typically found in recorded earthquakes must be considered in defining critical excitations. Accordingly, these authors suggested that the critical

excitations need to maximize, not only the structural response, but also, have to maximize the entropy rate. This was shown to lead to more realistic critical earthquake excitation models. In this paper, we reconsider the earlier proposition made by Manohar and Sarkar. Specifically, it is suggested that the actual entropy rates of earthquake records be estimated from available data and this information be used as an additional constraint in defining critical excitations. Here, it may be noted that, for a given frequency range (ω_0, ω_c), and for a given total average power, it can be shown that a band limited white noise would possess the highest entropy rate, and, conversely, a narrow band signal would possess the least entropy rate. A realistic ground motion, on the other hand, is unlikely to be an ideal band limited white noise nor an ideal narrow band signal. Consequently, the entropy rate associated with realistic ground motion is expected to be bounded between that of an ideal band limited white noise and of an ideal narrow banded signal. Thus, it can be expected that realistic models for critical seismic inputs be obtained by requiring that these inputs possess entropy rates that are actually observed in recorded ground motions. To do this, it is first noted that the entropy rate of a stationary, zero mean, Gaussian random process $\ddot{w}_g(t)$, in terms of its psd function $S(\omega)$, is given by [17]

$$\bar{H}_W = \log_e \sqrt{2\pi e} + \frac{1}{2(\omega_c - \omega_0)} \int_{\omega_0}^{\omega_c} \log_e S(\omega)\, d\omega \tag{21}$$

This equation can be used to estimate entropy rate from samples of Gaussian random processes. In the context of development of critical excitation models, it is found expedient to measure entropy rate with reference to a band limited white noise process $\ddot{\zeta}_g(t)$ with intensity I [3]. Under the assumption that $\ddot{w}_g(t)$ is independent of $\ddot{\zeta}_g(t)$, the increase in entropy rate when $\ddot{w}_g(t)$ is added to $\ddot{\zeta}_g(t)$ is given by

$$\Delta \bar{H}_W = \frac{1}{2(\omega_c - \omega_0)} \int_{\omega_0}^{\omega_c} \log_e \left[1.0 + \frac{S(\omega)}{I} \right] d\omega \tag{22}$$

Taking into account the discretization scheme used in this study (Equation (16)), $\Delta \bar{H}_W$ can be shown to be given by

$$\Delta \bar{H}_W = \frac{1}{2(\omega_c - \omega_0)} \sum_{n=1}^{N_f} (\omega_n - \omega_{n-1}) \log_e \left[1.0 + \frac{\sigma_n^2}{I(\omega_n - \omega_{n-1})} \right] \tag{23}$$

The problem of finding critical excitations can thus be stated as finding $\{\sigma_n^2\}_{n=1}^{N_f}$, that maximize

$$\max_{0 < t < \infty} \bar{\sigma}_k^2(t) = \max_{0 < t < \infty} \sum_{n=1}^{N_f} \sigma_n^2 H_k(\omega_n, t) \tag{24}$$

subjected to the constraints

$$\sum_{n=1}^{N_f} \sigma_n^2 = E_0; \quad \sum_{n=1}^{N_f} \sigma_n^2 \omega_n^2 = E_2$$

$$\frac{1}{2(\omega_c - \omega_0)} \sum_{n=1}^{N_f} (\omega_n - \omega_{n-1}) \log_e \left[1.0 + \frac{\sigma_n^2}{I(\omega_n - \omega_{n-1})} \right] \geqslant \Delta \bar{H}_W; \quad \sigma_n^2 \geqslant 0 \tag{25}$$
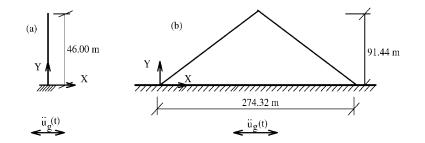
Figure 1. Example structures considered: (a) chimney [20], (b) Earth dam [21].

This problem, again, constitutes a constrained non-linear optimization problem. As in the previous case, the optimal solutions are computed using '*CONSTR*' program of the MATLAB Optimization Toolbox. Again, the optimization problem includes maximization across time as well as frequency domain (psd function). The steps of the maximization procedures are summarized as follows:

1. Compute $\{H_k(\omega_n, t_j)\}_{n=1}^{N_f}$, Equation (20), at a specific time $t = t_j$.
2. Calculate $\{\sigma_n^2\}_{n=1}^{N_f}$ that maximize response variance, $\bar{\sigma}_k^2(t_j)$.
3. Repeat steps 1 and 2 for all time points.
4. Estimate the maximum response variance $\bar{\sigma}_k^2(t_m) = \max \bar{\sigma}_k^2(t_j)$ and corresponding $\{\sigma_n^2\}_{n=1}^{N_f}$.
5. The estimated $\{\sigma_n^2\}_{n=1}^{N_f}$ define the critical psd function, Equation (16), and the corresponding critical response variance, Equation (19).

It is to be noted that the proposed procedure does not exclude the possibility of ground motions being narrow band in nature. If, indeed, at a given site, recorded motions exhibit highly resonant characteristics, the proposed procedure, in our study, would reflect this fact in the choice of the parameter n_0^+ as well as the constraint on entropy rate, $\Delta \bar{H}_W$.

4. NUMERICAL RESULTS AND DISCUSSIONS

Two example structures are considered for estimating the critical excitations (Figure 1). The first example is a tall reinforced concrete chimney representing a one-dimensional structure, while the second is an earth dam representing a two-dimensional structure. The two structures are assumed to be located at a firm soil site and are subjected to horizontal ground motion. The critical earthquakes are calculated for the two models developed in Sections 2 and 3. Additionally, for purpose of comparison, a third model which is based on earlier works [2, 4, 5] is also considered. In this model, the critical earthquake is assumed to be deterministic and is expanded as a linear summation in terms of normalized past recorded ground motions as follows:

$$\ddot{u}_g(t) = \sum_{n=1}^{N_r} a_n \ddot{\bar{v}}_{gn}(t) \tag{26}$$

Here $\{a_n\}_{n=1}^{N_r}$ are the variables of the optimization that are to be determined so that the response

$$\max_{0<t<\infty}|u_k(t)| = \max_{0<t<\infty}\left|\sum_{i=1}^{N}\sum_{n=1}^{N_r}\gamma_i\phi_{ki}a_n\int_0^t\ddot{v}_{gn}(\tau)h_i(t-\tau)\,\mathrm{d}\tau\right| \tag{27}$$

is maximized subjected to the constraints:

$$\left[\sum_{m=1}^{N_r}\sum_{n=1}^{N_r}a_m a_n\int_0^\infty\ddot{v}_{gm}(t)\ddot{v}_{gn}(t)\,\mathrm{d}t\right]^{1/2}\leqslant E_1$$

$$\max_{0<t<\infty}\left|\sum_{n=1}^{N_r}a_n\ddot{v}_{gn}(t)\right|\leqslant M_1$$

$$\max_{0<t<\infty}\left|\sum_{n=1}^{N_r}a_n\dot{v}_{gn}(t)\right|\leqslant M_2 \tag{28}$$

$$\max_{0<t<\infty}\left|\sum_{n=1}^{N_r}a_n\bar{v}_{gn}(t)\right|\leqslant M_3$$

This constitutes a non-linear constrained optimization problem is again solved using the same method that has been previously used for the first and second models. The critical excitations derived using Equation (26) are referred to as Model III in subsequent discussion.

4.1. Description of constraints

The implementation of the methods outlined in Sections 2 and 3 require, as a first step, quantification of the various constraints. To achieve this, a set of ten recorded earthquake ground motions has been selected [18, 19] (see Table I). The available records contain digitized information on acceleration, velocity and displacement. All these records are reported to have been measured on firm soil. Also, these ground motions have a minimum PGA of $0.27g$, and epicentral distance less than about 30 km. These ground motions were seen to produce similar Fourier spectra. Based on an analysis of these records we take $E_1 = 4.17\mathrm{m/s}^{1.5}$, $M_1 = 4.35$ m/s^2 $(0.44g)$, $M_2 = 0.60$ m/s, $M_3 = 0.15$ m. Figure 2 shows the plots of $M_4(\omega)$ and $M_5(\omega)$, which, respectively, are the upper and lower bounds on the Fourier amplitude spectra as defined in Equation (13). In the numerical calculations it is assumed that the frequency range of interest lies in 0.20–25.00 Hz. The envelope parameters are taken as $\alpha = 0.13$, $\beta = 0.50$ and $A_0 = 2.17$, which fix the duration of the critical earthquake to be about 30 s and maximum value of envelope $e(t)$ to unity. Similarly, the constraints that are relevant in deriving the stochastic critical excitations (Section 3) are taken to be $E_0 = 1.45$ m^2/s^4 and $n_0^+ = 1.64$ s^{-1}. The value of n_0^+ was selected based on the dominant frequency observed in Fourier transformation of recorded accelerograms. This value is consistent with the dominant frequency of 2 Hz that is prescribed for the Kanai–Tajimi spectra for a firm soil site [13]. This leads to $E_T = 11.40$ m^2/s^4 and $E_2 = 153.96$ m^2/s^6. Moreover, the assumed value for E_T implies that the expected PGA is about $0.44g$ which is same as the PGA used in the deterministic model.

The estimates of $\Delta\bar{H}_W$ obtained from individual records is also listed in Table I. Here, the intensity of the reference white noise $\ddot{\zeta}_g(t)$ is taken to be $0.02\,\mathrm{m}^2/\mathrm{s}^3$. In estimating $\Delta\bar{H}_W$, each

Table I. Information on basis earthquake records for a firm soil site [18, 19].

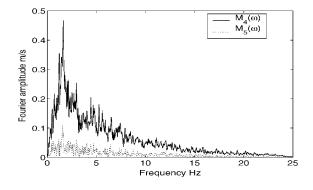| SNo.	Earthquake	Site	Magni-tude	Epicentral distance (km)	Compo-nent	PGA (m/s^2)	PGV (m/s)	PGD (m)	Inten-sity (m/s$^{1.5}$)	$\Delta \bar{H}_W$
1	Mamoth lakes 05.25.1980	Convict Greek	6.2	1.5	W	4.02	0.21	0.05	3.73	0.6164
2	Loma prieta 10.18.1989	Capitola	7.0	9.7	W	3.91	0.31	0.07	3.82	0.6307
3	Morgan hill 04.24.1984	Halls valley	6.1	4.5	S60E	3.06	0.40	0.07	2.33	0.6276
4	San Fernando 02.09.1971	Castaic, old ridge route	6.6	27.6	N21E	3.09	0.17	0.04	2.07	0.6158
5	Parkfield 12.20.1994	Parkfield fault zone	5.0	9.1	N	3.80	0.10	0.01	1.74	0.6358
6	Caolinga 05.02.1983	Cantua creek school	6.5	30.1	N	2.83	0.26	0.10	2.67	0.6168
7	Northridge 01.17.1994	Canoga park	6.7	5.9	S16W	3.81	0.60	0.12	4.17	0.6303
8	Cape Mendocino 04.25.1992	Petrolia general store	7.0	5.4	N	3.25	0.45	0.15	2.44	0.6256
9	Westmorland 04.26.1981	Westmorland fire station	5.0	6.6	S	4.35	0.44	0.15	3.26	0.6171
10	Imperial valley 10.15.1979	Calexico fire station	6.4	17.4	S45W	2.68	0.22	0.10	2.30	0.6369

Figure 2. Upper and lower bound Fourier amplitude spectra constraints.

record is assumed to be representable in the form of Equation (3). An estimate of the envelope of the form given in Equation (5) is obtained by selecting A_0, α and β to match the transient trend of the earthquake record. Subsequently, samples of the stationary part of acceleration, namely $\ddot{w}_g(t)$ are obtained by dividing the given record by the estimated envelope. This is followed by estimation of sample psd of $\ddot{w}_g(t)$ which, in conjunction with Equation (22), leads to the estimate of $\Delta \bar{H}_W$. As can be seen from Table I, the average value of $\Delta \bar{H}_W$

Earthquake Engng Struct. Dyn. 2002; **31**:813–832

Table II. Nomenclature combinations of constraints used for Model I: Deterministic model of Section 2; Model II: Stochastic model of Section 3 and Model III: Data based model of Section 4.

Case	Model I	Model II	Model III
1	Intensity & PGA	E_T & n_0^+	Intensity & PGA
2	Intensity, PGA & UBFAS	E_T, n_0^+ & $\Delta\bar{H}_W$	Intensity, PGA, PGV & PGD
3	Intensity, PGA, PGV, PGD & UBFAS	—	—
4	Intensity, PGA, UBFAS & LBFAS	—	—

across the ten records turns out to be about 0.63. For sake of comparison, the increase of entropy rate $\Delta\bar{H}_W$ was also computed for a Kanai–Tajimi psd valid for firm ground, that is, with soil natural frequency $\omega_g = 2.50$ Hz, soil damping $\eta_g = 0.60$ and intensity parameter $0.02 \, \text{m}^2/\text{s}^3$ [13]. This value was computed to be 0.64, which is close to the value estimated for the recorded ground motions in Table I.

4.2. Example 1: seismic response of a chimney

A 46 m tall reinforced concrete chimney with a uniform circular cross-section, of 3.80 m outer diameter, 3.30 m inner diameter, constant mass density of 2500 kg/m^3 and modulus of elasticity $E = 2.0 \times 10^{10}$ N/m^2 [20] is considered (Figure 1(a)). A finite element analysis using 20 two-noded beam elements, with one translational and one rotational degree of freedom at each node, showed that the first five natural frequencies of the chimney were $0.94, 5.90, 16.52, 32.36$ and 53.51 Hz, respectively. Since only the first three modes lie in the assumed frequency range of 0.20–25.00 Hz, we retain only the first three modes in the subsequent analysis. A modal viscous damping of 5 per cent was assumed for all the three modes.

A detailed parametric study involving three response variables (tip relative displacement, base bending moment and base shear force) and different combinations of constraints has been conducted with an aim to discern characteristics of associated critical excitations and the highest responses. The nomenclature used for describing various models and the constraint combinations considered is summarized in Table II. As has been already mentioned, the optimization problems in developing Models I, II and III have been tackled by using '$CONSTR$' program of MATLAB Optimization Toolbox. While implementing this procedure, several alternative starting solutions from within the feasible region were considered and it was observed that all the starting solutions lead to the same maximum. The question of number of terms to be retained on the series representations used in Model I (Equation (4)) and Model II (Equation (16)) on the convergence of critical response was considered first. In either case, about 30 terms were found to give satisfactory representation. It is to be noted here that in distributing $\{\omega_n\}_{n=1}^{N_f}$ in the interval (ω_0, ω_c), it was found advantageous to select some of these ω_n to coincide exactly with the structure natural frequencies that lie in (ω_0, ω_c) and also to place relatively more points within the modal half-power bandwidths. In the subsequent numerical work it is assumed that $N_f = 31$.

The effect of imposing alternative constraints on the critical excitations (Model I) is studied. Figures 3 and 4 show the critical excitations and their Fourier amplitude spectra for cases 3
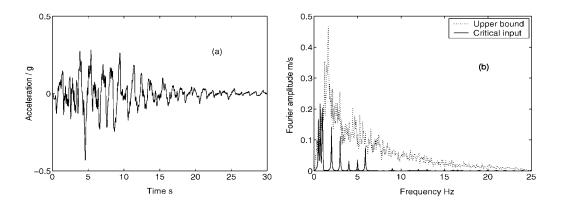
Figure 3. Example 1: Critical ground acceleration, Model I, case 3; (a) Time
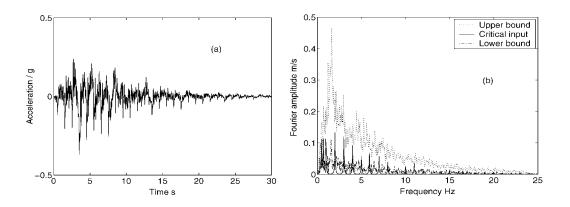history (b) Fourier amplitude spectrum.

Figure 4. Example 1: Critical ground acceleration, Model I, case 4; (a) Time
history (b) Fourier amplitude spectrum.

and 4, respectively. Here, the response variable to be maximized is taken to be the tip relative
displacement of the chimney. Given the series representation adopted for critical excitations,
see Equation (4), the imposition of constraints on lower and upper bound Fourier amplitude
spectra, has been possible only at discrete frequencies given by $\omega = \omega_n$, $n = 1, 2, \ldots, N_f$. Re-
sults from stochastic critical excitation models are shown in Figure 5 for case 2. Here again
the critical response is the standard deviation of the tip relative displacement. The results on
critical responses are summarized in Tables III and IV. Table III gives the maximum dis-
placements corresponding to constraint cases 1−4 for Model I. The highest bending moment
and shear force at the base that the corresponding critical excitations produce are also listed
in this table. Similar results obtained using Models II and III are shown in Table IV. For
purpose of comparison, the chimney responses to the recorded earthquake inputs $\{\ddot{v}_{gn}(t)\}_{n=1}^{N_r}$
were also computed. It was found that the highest tip relative displacement, base bending
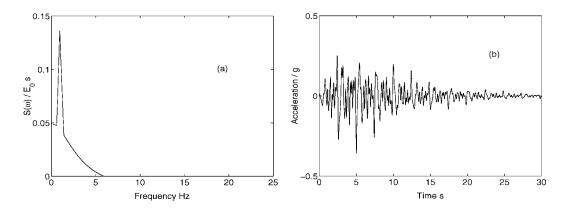
Earthquake Engng Struct. Dyn. 2002; **31**:813–832

Figure 5. Example 1: (a) psd of $\ddot{w}_g(t)$, (b) sample realization of critical $\ddot{u}_g(t)$, Model II, case 2.

Table III. Summary of maximum responses for Model I: (a) chimney (response variable is tip relative displacement), (b) Earth dam (response variable is horizontal tip displacement).

Case	Chimney response			Earth dam response	
	u_{max} (m)	BM_{max} (MN m)	SF_{max} (MN)	$u_{x_{max}}$(m)	$u_{y_{max}}$(m)
1	0.8520	125.0811	3.7516	0.5357	0.0365
2	0.6348	92.1632	2.8706	0.5353	0.0366
3	0.5489	80.5604	2.5755	0.4863	0.0401
4	0.3475	50.0173	1.6672	0.2895	0.0493

moment and base shear force were, respectively, 0.2067 m, 30.2081 MN m and 1.0728 MN. Based on the extensive numerical investigations carried out and based on results presented in Figures 3–5 and Tables III and IV, the following observations are made

1. For Model I, the magnitude of critical response produced and frequency content of critical excitations are strongly dependent on constraints imposed (Figures 3 and 4, Table III). If available knowledge on future earthquake is limited to its intensity and PGA (case 1), the critical excitations are highly resonant and response produced is overly conservative (Table III). Additional constraints on bounds on Fourier amplitude spectra (case 4) makes the critical excitations realistic in terms of their frequency content and the responses that they produce. To see this, the critical responses produced by alternative constraint scenarios can be compared with the highest tip relative displacement of 0.2067 m that is produced by the recorded motions $\{\ddot{v}_{gn}(t)\}_{n=1}^{N_r}$. Thus for the case of constraints on intensity and PGA (case 1), the critical response is 4.12 times the highest response produced by $\{\ddot{v}_{gn}(t)\}_{n=1}^{N_r}$ while, for case 4 this ratio is about 1.68.

2. Similar feature is also observed in Model II, where imposition of constraints on input entropy rate makes the critical psd non-resonant in nature. Subsequently, the critical response, namely the standard deviation of tip displacement, drops from a value of 0.41 to 0.24 m as the constraint on entropy rate is brought in.

Table IV. Maximum responses for the chimney for alternative critical response variables.

Response variable	Model I, case 4			Model II, case 2			Model III, case 1		
	u_{max} (m)	BM_{max} (MN m)	SF_{max} (MN)	$\bar{\sigma}_{u_{max}}$ (m)	$\bar{\sigma}_{BM_{max}}$ (MN m)	$\bar{\sigma}_{SF_{max}}$ (MN)	u_{max} (m)	BM_{max} (MN m)	SF_{max} (MN)
Displacement	0.3475	50.0171	1.6672	0.2440	35.8112	1.07680	0.3668	53.3102	1.5866
Bending moment	0.3396	53.6852	1.8910	0.2440	35.8223	1.07680	0.3650	53.5263	1.6190
Shear force	0.3340	53.1140	1.9068	0.2439	35.8141	1.07690	0.3526	52.4934	1.6549

Table V. Summary of changes in maximum responses for the chimney due to changes in constraints and envelope parameters.

Model	Model I, cases 3 & 4									Model II, case 2			
Parameter	E_1	M_1	M_2	M_3	$M_4(\omega)$	$M_5(\omega)$	α	β	E_T	n_0^+	$\Delta\bar{H}_W$	α	β
ε_1	0.17	0.06	0.04	0.03	0.04	0.02	0.03	0.06	1.44	0.48	2.34	0.04	0.10
ε_2	0.014	0.005	0.023	0.070	0.029*	0.063*	0.080	0.041	0.031	0.071	0.017	0.075	0.049

*Note that values reported here represent ε_2 at the frequency at which $M_4(\omega)$ and $M_5(\omega)$ are at respective maxima.

3. The imposition of constraints on bounds on Fourier amplitude spectra in Model I and on the entropy rate in Model II, essentially force the input energy to get redistributed at frequencies other than the structure fundamental frequency. In Model I, it was observed that the Fourier coefficients at the first two modes reach their respective upper bounds and the energy also gets distributed across other frequencies that are not the structure frequencies. On the other hand, for Model II, upon imposition of a constraint on entropy rate, the critical psd continues to possess a dominant peak at the structure fundamental mode but with significant average power smeared across other frequencies with no bias at higher structure natural frequencies.

4. In the numerical studies, it was observed that the qualitative nature of critical inputs did not change as alternative critical response variables, namely, tip relative displacement, base bending moment and base shear force were considered. This is to be expected, given the one dimensional nature of the structure. Here, all the three response variables considered are likely to be dominated by the fundamental mode. Table IV summarizes the maximum values of critical responses produced by Models I, II and III as the critical response variables are varied. It is to be noted that results from Model II refer to the highest standard deviations. It can be seen that the responses produced by Model I (case 4) compare well with corresponding results from Model III. To compare the results from Model II with those from deterministic models, one has to multiply results from Model II by a peak factor before this comparison can be carried out. An approximate analysis, with an assumed duration of 30 s, revealed a peak factor of about 2.70. Based on this, results from Model II with constraints on intensity and entropy rate, are seen to produce relatively higher responses.

With a view to understand the sensitivity of critical response with respect to variations in values of constraints, as well as variations in values of envelope parameters, a limited amount of sensitivity analyses using numerical methods have been carried out. For this purpose both deterministic model (Model I) and stochastic model (Model II) are considered. The parameters in Model I are E_1, M_1, M_2, M_3, $M_4(\omega)$, $M_5(\omega)$, α and β, while for Model II, the parameters are E_T, n_0^+, α and β. To study the sensitivity of critical response with respect to a specific parameter, the value of this parameter is changed by 1 per cent while all other parameters are held fixed at their respective specified values. The optimization problem is re-solved with this change in place. This leads to the calculation of the percentage change in the critical response, denoted by ε_1, and also the ratio of change in the response value to the change in the parameter value, denoted by ε_2. Table V summarizes the results of this calculation for the cases of critical responses being the tip relative displacement and the standard deviation of the tip relative displacement for Models I and II, respectively. For the bounds $M_4(\omega)$ and $M_5(\omega)$, the change of 1 per cent is taken to be uniform across all frequencies. In the deterministic model, the results presented in Table V corresponding to M_2 and M_3 are for case 3, while others correspond to case 4 of the same model. Results of stochastic model correspond to case 2. It can be observed from Table V that the change in intensity parameter, E_1, and LBFAS, $M_5(\omega)$, for Model I, alters the optimum solution considerably compared to similar changes in other parameters. For the stochastic model, entropy rate, $\Delta \bar{H}_W$ and intensity, E_T, produce noticeable changes in the optimum solution compared to changes in other parameters. The optimum solution is less sensitive to the envelope parameters, α and β for both the models.
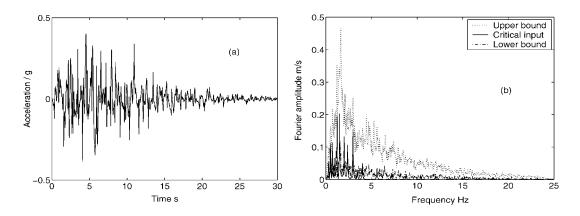
Figure 6. Example 2: Critical ground acceleration, Model I, case 4; (a) Time history (b) Fourier amplitude spectrum, response variable is horizontal tip relative displacement.
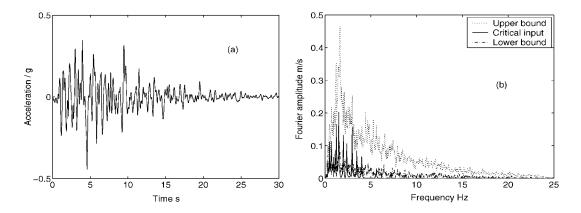

Figure 7. Example 2: Critical ground acceleration, Model I, case 4; (a) Time history (b) Fourier amplitude spectrum, response variable is vertical tip displacement.

4.3. Example 2: seismic response of an earth dam

The dam structure considered has modulus of elasticity $E = 8.09 \times 10^{10}$ N/m^2, mass density of 1.84×10^8 kg/m^3 and Poisson's ratio $v = 0.45$ (Figure 1(b)). The seismic response of this structure has been considered earlier by Clough and Chopra [21]. The dam is modelled using seven 2-D, plane strain, eight-noded, quadrilateral elements with two translational degrees of freedom at each node. Free vibration analysis is carried out using NISA finite element package and the first five natural frequencies were found to be 1.24, 1.99, 2.37, 2.97 and 3.47 Hz, respectively. These values match well with those presented in Reference [21]. Only the first five modes are considered in the subsequent analysis and modal damping is assumed to be 5 per cent for all the five modes.
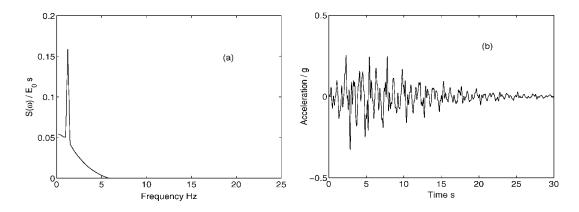
Figure 8. Example 2: (a) psd of $\ddot{w}_g(t)$, (b) sample realization of critical $\ddot{u}_g(t)$, Model II, case 2, response variable is horizontal tip relative displacement.
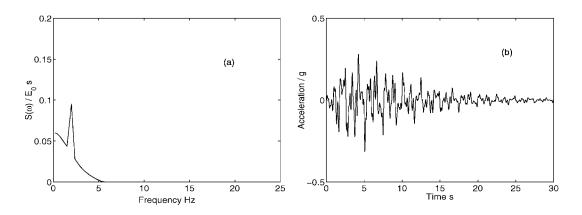

Figure 9. Example 2: (a) psd of $\ddot{w}_g(t)$, (b) sample realization of critical $\ddot{u}_g(t)$, Model II, case 2, response variable is vertical tip displacement.

The critical excitations, as per Models I, II and III, and for alternative scenarios listed in Table II were studied for this structure also. The nature of dependence of critical input and the responses on alternative constraint scenarios was broadly similar to the one observed in the previous example. However, given the two-dimensional nature of the earth dam structure, it may be expected that alternative response variables, such as horizontal tip displacement and vertical tip displacement, are dominated by distinct structure modes. Consequently, the nature of critical inputs for these alternative response variables can be expected to be different from each other. This is illustrated in Figures 6–9, in which results on critical inputs for Models I and II are presented for the cases of two critical response variables, namely, tip horizontal displacement and tip vertical displacement. It may be observed from Figures 6(b), 7(b), 8(a) and 9(a) that the frequency content of critical input change noticeably as the response variable is changed from tip horizontal displacement to tip vertical displacement. The results on the

Table VI. Maximum responses for the earth dam for alternative critical response variables.

Response variable	Model I, case 4		Model II, case 2		Model III, case 1	
	$u_{x_{max}}$ (m)	$u_{y_{max}}$ (m)	$\bar{\sigma}_{x_{max}}$ (m)	$\bar{\sigma}_{y_{max}}$ (m)	$u_{x_{max}}$ (m)	$u_{y_{max}}$ (m)
Horizontal displacement	0.2895	0.0493	0.1154	0.0224	0.3292	0.0586
Vertical displacement	0.1784	0.0720	0.0835	0.0300	0.1613	0.0801

critical responses produced are summarized in Table VI. The highest horizontal and vertical tip displacement produced by $\{\ddot{v}_{gn}(t)\}_{n=1}^{N_r}$ were, respectively found to be 0.1946 and 0.0531 m. The critical responses for Model I case 4 is seen to compare well with results from Model III case 1. While responses from Model II case 2, are seen to be higher. Again, it has to be noted that results from model II are to be multiplied by a peak factor of 2.7 before these results can be compared with results from Models I and III. Detailed study on Model I, for constraints as in cases 1–4 (Table II) was also carried out and the critical responses produced are summarized in Table III. The qualitative trends observed here were similar to the one observed in the previous example. The highest horizontal displacement corresponding to Model I case 1 is observed to be 2.75 times the highest response produced by $\{\ddot{v}_{gn}(t)\}_{n=1}^{N_r}$, while for vertical displacement this ratio is 2.21. For case 4, these ratios drop to 1.49 and 1.36 for horizontal and vertical displacements, respectively.

5. CONCLUDING REMARKS

Critical seismic excitations, by definition, depend upon reliably known features of earthquake and on dynamic characteristics of the structure under consideration. The dependence of these excitations on structure properties introduces elements of artificialness into their characteristics. The realism contained in critical excitations is dependent on the set of constraints that these excitations are required to satisfy. The present study has explored the dependence of the nature of critical excitations on a set of constraints that reflect intensity, peak values of ground acceleration, velocity and displacement, upper and lower bounds on Fourier amplitude spectra and measures of disorder expressible in terms of input entropy rate. Studies within the frameworks of deterministic and stochastic analysis have been reported. The illustrative examples include a one-dimensional and a two-dimensional structures. Based on this study, we reach the conclusion that the constraints involving lower and upper bound on Fourier amplitude spectra for deterministic models and constraints on entropy rate for stochastic models are crucial in developing realistic critical excitation models.

REFERENCES

1. Drenick RF. Model-free design of aseismic structures. *Journal of Engineering Mechanics* 1970; **96**:483–493.
2. Drenick RF. Aseismic design by way of critical excitation. *Journal of Engineering Mechanics* 1973; **99**: 649–667.
3. Manohar CS, Sarkar A. Critical earthquake input power spectral density function models for engineering structures. *Earthquake Engineering and Structural Dynamics* 1995; **24**:1549–1566.

4. Wang PC, Yun CB. Site-dependent critical design spectra. *Earthquake Engineering and Structural Dynamics* 1979; **7**:569–578.
5. Bedrosian B, Barbela M, Drenick RF, Tsirk A. Critical excitation method for calculating earthquake effects on nuclear plant structures: An assessment study. *NUREG/CR-1673*, *RD*, *U.S. Nuclear regulatory commission*, *Burns and Roe, Inc.*, Oradell, NJ, 1980.
6. Srinivasan M, Corotis R, Ellingwood B. Generation of critical stochastic earthquakes. *Earthquake Engineering and Structural Dynamics* 1992; **21**:275–288.
7. Shinozuka M. Maximum structural response to seismic excitations. *Journal of Engineering Mechanics* 1970; **96**:729–738.
8. Iyengar RN, Manohar CS. Nonstationary random critical excitations. *Journal of Engineering Mechanics*, 1987; **133**:529–541.
9. Sarkar A, Manohar CS. Critical cross power spectral density functions and the highest response of multi-supported structures to multi component earthquake excitations. *Earthquake Engineering and Structural Dynamics* 1996; **25**:303–315.
10. Sarkar A, Manohar CS. Critical seismic vector random excitations for multi-supported structures. *Journal of Sound and Vibration* 1998; **212(3)**:525–546.
11. Takewaki I. Optimal damper placement for critical excitation. *Probabilistic Engineering Mechanics* 2000; **15**:317–325.
12. Takewaki I. A new method for non-stationary random critical excitation. *Earthquake Engineering and Structural Dynamics* 2001; **30**:519–535.
13. Clough RH, Penzien J. *Dynamics of Structures* (2nd edn). McGraw-Hill: Tokyo, 1993.
14. Shinozuka M, Sato Y. Simulation of nonstationary random process. *Journal of Engineering Mechanics* 1967; **91**:11–40.
15. Shinozuka M, Henry L. Random vibration of a beam column. *Journal of Engineering Mechanics* 1965; **91**: 123–143.
16. Baratta A, Elishakoff I, Zuccaro G, Shinozuka M. A generalization of the Drenick–Shinozuka model for bounds on the seismic response of a single-degree-of-freedom system. *Earthquake Engineering and Structural Dynamics* 1998; **27**:423–437.
17. Papoulis A. *Probability*, *Random Variable and Stochastic Processes*. McGraw-Hill: New York, 1991.
18. Shakal AF, Huang MJ. Standard tape format for CSMIP strong-motion data tapes. California strong motion instrumentation program. *Report OSMS 85-03*, 1985.
19. SMDB. The Strong Motion Databased. *http://smdb.crustal.ucsb.edu/*, Southern California Earthquake Center, 2000.
20. Pinfold GM. *Reinforced Concrete Chimneys and Towers*. Viewpoint Publications: London, 1975.
21. Clough RW, Chopra AK. Earthquake stress analysis in earth dams. *Journal of Engineering Mechanics* 1966; **92**:123–143.